Mesoporous and Amorphous NiCoBP Alloys with High Specific Capacitance for Supercapacitors

Qian Ren[1], Shan Ji[2,], Dan Brett[2], Bruno G. Pollet[3], Hui Wang[1]and Rongfang Wang[1,]

1. College of Chemistry and Chemical Engineering, Northwest Normal University, Lanzhou 730070, China

2. Electrochemical Innovation Lab, Dept. Chemical Engineering, University College London, London, WC1E 6BT, UK

3. Eau2Energy, Nottingham NG14 6DX, England, UK

Abstract: A facile and versatile low cost solid-liquid interface-mediated method for the synthesis of mesoporous and amorphous NiCoBP alloys possessing high surface areas was developed. The precursors of Ni, Co and P, with controllable molar ratio, were first dissolved in ultrapure water, frozen and treated with $NaBH_4$ solution to form NiCoBP alloys at room temperature. Benefiting from its mesoporous and amorphous structural features, the *as*-prepared NiCoBP alloy exhibited high surface area and exceptional electrochemical performance for use as a cathode material in asymmetric supercapacitors, yielding specific capacitance of up to 1030.4 F g^{-1} at 6 A g^{-1} with excellent cycling stability.

Keywords: Amorphous; NiCoBP alloy; Mesoporous; Cathode; Supercapacitor

R

1. Introduction

Supercapacitors have attracted considerable research interest as they are promising electrochemical energy storage devices, especially for the portable electronic and electric vehicle sectors, due to their high reliability, long cycle life and high power/energy density [1, 2]. Generally, the performance of supercapacitors depends upon the selected electrode materials employed, which are usually divided into three categories, namely: (i) carbonaceous materials with high stability and electronic conductivities, but with low specific capacitances; (ii) conductive polymers with high specific capacitances, but with poor cycling stability and (iii) transition metal oxides with high specific capacitances and stability, but with poor electronic conductivities [3, 4].

Based on the fast and reversible redox reactions which occur on the active material surfaces, the transition metal oxides have been found to be promising electrode materials for supercapacitors due to their larger capacitances and energy densities [5]; however, their electronic conductivities require further improvement. For example, high conductive carbon materials mixed with transition metal oxides usually improve the electrochemical performance of the active electrode materials. Chidembo and co-workers [6] reported the use of a spray pyrolysis method to synthesize high surface area, self-organized, micron-sized 'urchin-like' composites, made up of reduced graphene oxide and needle-shaped Mn_2O_3-Mn_3O_4; these materials exhibited maximum capacitances of 425 F g^{-1} at 5 mV s^{-1} and 133 F g^{-1} at a current density of

0.2 A g^{-1}. Jiang *et al.* [7] prepared powdery carbon@MnO_2 core-shell hybrid nano-spheres used as supercapacitor electrode materials, in which the core carbon spheres served as a supporting template and electronically conductive material for the nanostructured MnO_2 shell. Currently, the development of new electrode materials for *pseudo* capacitors, using high performance and low cost transition metal oxides, is still regarded as an important area of research.

Amorphous metal alloys are a type of metastable material consisting of irregular shaped and broad size distributed particles with long-range disordered and short-range ordered structures. Due to their homogeneous single-phase nature (i.e. the absence of chemical and physical heterogeneity), when compared to their crystalline counterparts, amorphous metal alloys exhibit superior corrosion resistance, high mechanical toughness, and excellent magnetic, electronic, and catalytic properties [8-10]. Among these amorphous alloys, metal borides have been thoroughly studied [11-13]. For example, Zhao *et al.* [9] prepared amorphous NiB and NiMnB alloy nanoparticles and applied the materials as *pseudo* capacitor electrodes. The authors showed that NiB and NiMnB electrodes could achieve a specific capacitance of up to 562 and 768 F g^{-1}, respectively. Ternary MgCoB alloys exhibiting good electrochemical reversibility and high specific capacitance values for alkaline secondary batteries were successfully synthesized by a chemical reduction method, with subsequent heat-treatment at various temperatures [12]. Although previous studies showed metal borides of good electrochemical properties, their specific capacitances and charge-discharge lifespans were still not acceptable for practical applications.

Phosphorous is well-known to be a non-metallic element with five valence electrons which can form stable amorphous metal-phosphorous alloys [5, 14-16]. In this paper, we build on the advantages of amorphous NiCoB and further modify the alloy by using a low cost, solid-liquid, interface-mediated method to yield amorphous NiCoBP alloys with high surface areas. Compared to amorphous NiCoB alloys, the *as*-prepared NiCoBP particles showed excellent supercapacitive performance in terms of high specific capacitance, long charge-discharge lifespan and remarkable rate capability. It is suggested that the improved electrochemical performance could be contributed to the high surface area and the introduction of phosphorous.

2. Experimental

2.1 Synthesis and characterization of amorphous NiCoBP and NiCoB alloys

All reagents were of Analytical Grade and ultrapure water was used throughout the experiments. The preparation of amorphous NiCoBP alloy is as follows: 100 mg of $NiCl_2$, 100 mg of $CoCl_2$ and 45 mg of NaH_2PO_2 were added into 25 mL of ultrapure water in a 100 ml beaker. The solution was refrigerated and frozen at -20^{o}C for 12 h. 25 mL of 0.08 mol L^{-1} $NaBH_4$ was slowly poured onto the frozen solution. After that, the beaker was sealed with Parafilm and kept at room temperature for 8 h. The product was then collected by centrifugation and washed thoroughly, alternating between water and ethanol for several times before drying at 60^{o}C for 12 h. For comparison, amorphous NiCoB alloys were prepared using a similar procedure, whereby NiCoBP was prepared without the addition of NaH_2PO_2.

2.2 Characterization

All XRD patterns were recorded on a Shimadzu XD–3A (Japan) using filtered Cu-Kα radiation (λ = 0.15418 nm) generated at 40 kV and 30 mA. Scans for 2θ values were recorded at 4°min^{-1}. Scanning electron microscopy (SEM) images were obtained using a Carl Zeiss Ultra Plus. Transmission electron microscopy (TEM) images, selected area electron diffraction (SAED) patterns and energy dispersive spectroscopy (EDS) of the electrode materials were obtained using a JEOL (JEM-2000 FX) microscope operating at 200 kV. The sorption isotherms were obtained on a Quantachrome Autosorb-1 volumetric analyser. Specific surface areas were determined by the Brunauer-Emmett-Teller (BET) method and the pore size distribution (calculated from the desorption part of the nitrogen sorption isotherms based on Barrett-Joyner-Halenda (BJH) theory) was determined from the meso- and macro-range of pore size distribution.

2.3 Electrochemical measurements.

Cyclic voltammetry (CV) and galvanic charge/discharge cycling methods were used to evaluate the electrochemical behavior of the *as*-prepared alloy samples in a three-electrode cell system. The working electrode was fabricated using a homogeneous 'dough' of alloys, carbon black and poly(tetrafluoroethylene) with a mass ratio of 80:10:10 in isopropanol, that was rolled to an uniform film thickness (~100 μm) and dried at 80°C for 6 h. Film slices were pressed onto the stainless steel grids (1 cm × 1 cm) using a tablet press. The reference electrode was an Hg/HgO (1.0 M K_2SO_4) electrode. The electrolyte was 6.0 mol L^{-1} KOH. CV tests were carried out over a potential range of -0.2 to +0.5 V *vs*. Hg/HgO at different scan rates (5, 10, 30,

50 and 100 mV s^{-1}) using a CHI 650D electrochemical workstation. Galvanic charge/discharge and cycle life tests were carried out on a Neware Battery Tester (BTS6.0, Neware Technology Company, Guangdong, China).

3. Results and discussion

Interfacial interactions can be used for the 'controlled' growth of various nanostructures, which are mainly formed by self-aggregation driven by the two-phase interface [10, 17, 18]. At the interface of the two phases, reactants are more prone to react with the surrounding species and to produce many useful properties [19]. In this paper, we demonstrate a facile method for the synthesis of NiCoB and NiCoBP alloys at the interface of a liquid-solid phase. Figure 1 shows the XRD patterns of the *as*-prepared NiCoB and NiCoBP alloys. The figure does not show any sharp peaks related to the periodic lattice, apart from the very weak and featureless XRD patterns, indicating that NiCoB and NiCoBP reduced by $NaBH_4$ on the interface of the liquid-solid phase have amorphous crystalline structures [11, 16]. Both samples show a weak and broad diffraction peak at ca. $2\theta = 45^{o}$ in the XRD patterns, which also confirms the amorphous nature of the two samples [9, 20].

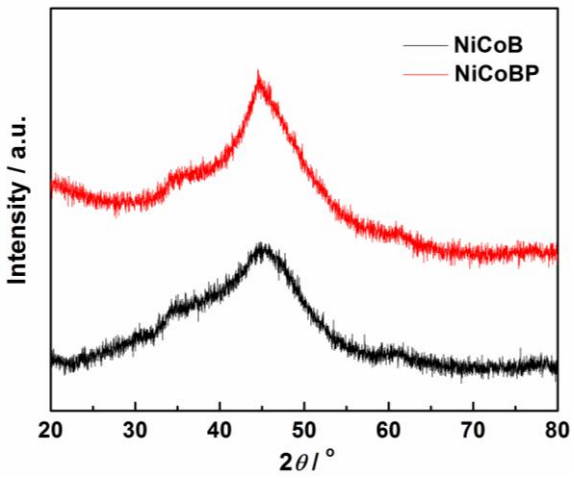

Figure 1 XRD patterns of NiCoB and NiCoBP alloys.

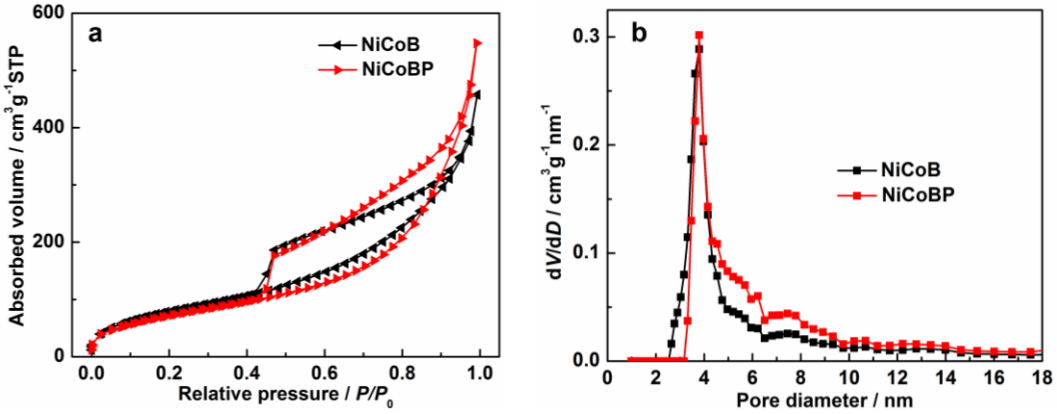

Figure 2 N_2 adsorption-desorption isotherms (a) and pore size distribution (b) of NiCoB and NiCoBP.

The BET surface area and porous structure of the *as*-prepared amorphous NiCoB and NiCoBP alloys were characterised by the adsorption-desorption isotherms of N_2 at -196^{o}C and shown in Figure 2. Both isotherms belong to mixed types in the *IUPAC* classification, namely *type I* at low relative pressures and *type IV* at intermediate and high relative pressures. At the low relative pressure region, they are of *type I* with a clear uptake which is characteristic of microporous materials. At the relative pressure, there is a certain hysteresis slope, indicating the presence of large micropores and mesopores [21]. The BET surface areas of NiCoB and NiCoBP were found to be 286.02 and 257.71 m^2g^{-1} respectively, indicating that the surface area is slightly decreased by the introduction of phosphorous into the NiCoB alloy structure. As shown in Figure 2(b), the pore distribution of both samples are centered at 4.5 nm, suggesting that mesoporous alloys were formed.

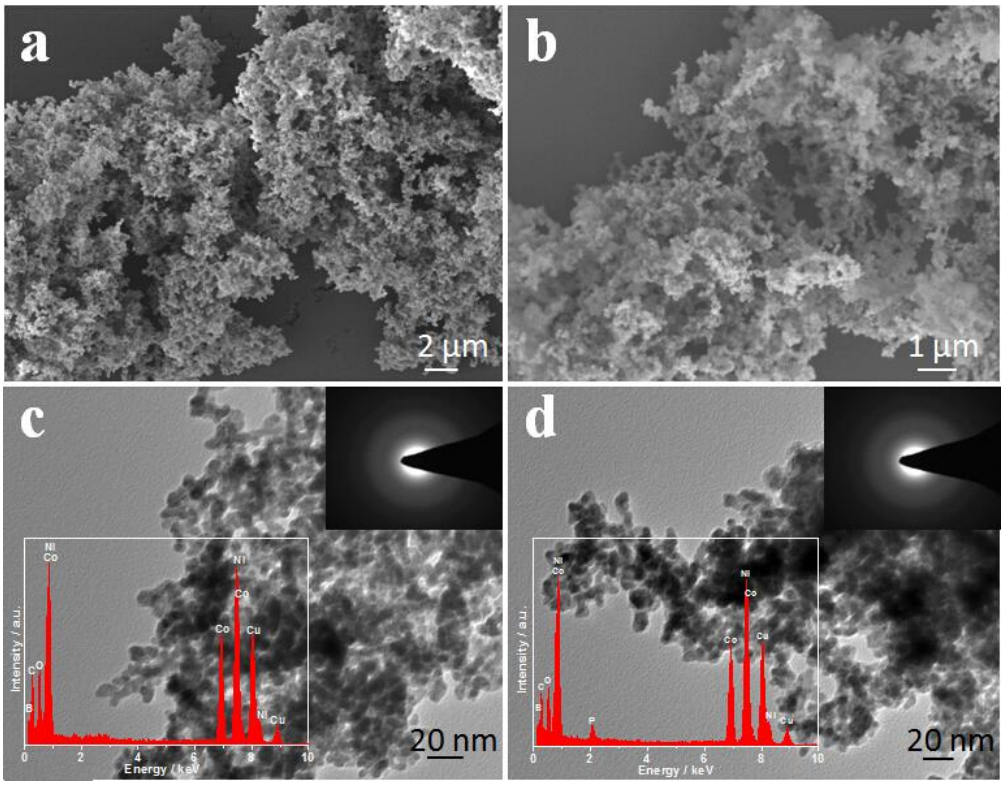

Figure 3 SEM images of NiCoB (a) and NiCoBP (b) alloys; TEM and SAED images of NiCoB (c) and NiCoBP (d) alloys.

Figures 3(a) and 3(b) show SEM images of NiCoB and NiCoBP alloys. SEM images clearly indicate that the *as*-prepared NiCoB and NiCoBP alloys have almost identical morphologies, consisting of an extensive network-like structure of aligned nanoparticles. This structure was also visible in TEM images, as shown in Figures 3(c) and 3(d). The TEM images clearly show that most particles had elliptical shape with diameter of 5-10 nm. The insets at the upper right corner in Figure 3(c) and 3(d) presents the SAED of the two samples. A continuous hollow ring which is a typical diffraction pattern of an amorphous material can be observed, further confirming the amorphous structure of NiCoB and NiCoBP. The compositions of the two samples were determined by EDS analysis, as displayed in the lower left corner of Figure 3(c)

and 3(d). The Ni:Co:B(:P) atomic ratio of NiCoB and NiCoBP is 1:1:0.20 and 1:1:0.22 respectively:

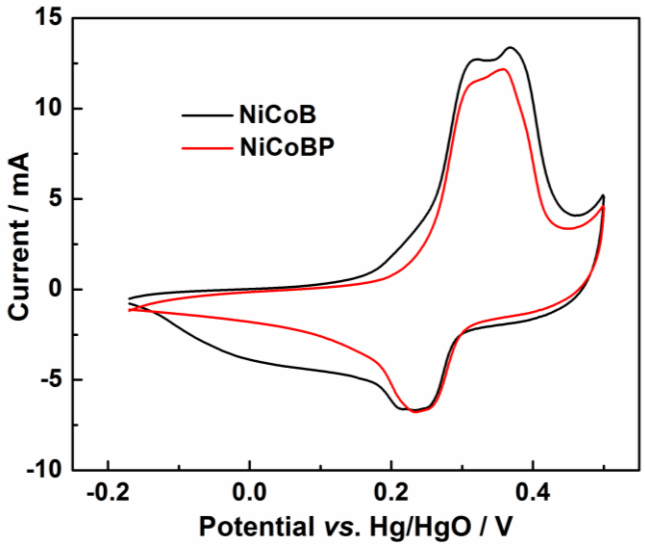

Figure 4 Cyclic voltammograms of NiCoB and NiCoBP electrodes at scan rate of 5 mV s^{-1} in 6 M KOH.

The study then turned to the electrochemical characterisation of the fabricated alloys. The *as*-prepared NiCoB and NiCoBP alloys were mechanically mixed with carbon black and PTFE solution to yield a paste which was loaded onto a current collector to form a supercapacitor cathode. The electrochemical performance of the *as*-prepared electrode was evaluated by CV and galvanostatic charge-discharge tests in a three-electrode cell. Figure 4 shows a typical CV curve of the NiCoB and NiCoBP at a scan rate of 5 mV s^{-1} in the potential range from -0.2 to +0.5 V (*vs.* Hg/HgO). The obtained CV curves show typical *pseudo* capacitive characteristics; in other words, two pairs of strong redox peaks are present in both CV curves, which are mainly attributed to the Faradaic redox reaction of M-O/M-OOH (M = Ni and Co) in the alkaline electrolyte (KOH). The redox reactions in the KOH background

electrolyte could be contributed to the conversion reactions occurring in the NiCo-based alloy, as shown in the following reactions [22-24]:

$$NiCo + OH^- + H_2O \longleftrightarrow NiOOH + CoOOH + 2e^- \quad (1)$$

$$CoOOH + OH^- \longleftrightarrow CoO_2 + H_2O + e^- \quad (2)$$

Compared to the CV curve for the NiCoB alloy shown in Figure 4, the voltammetric currents of NiCoBP are lower, which may result from the smaller BET surface area after phosphorous was introduced into NiCoBP. When the scan rate increases from 5 mV s^{-1} to 100 mV s^{-1}, two pairs of redox peaks are visible in all the CV curves (Figure 5). The gaps between the redox peaks (ΔE_p) at a scan rate of 5 mV s^{-1} becomes wider with increased anodic and cathodic current responses when the scan rate increases to 100 mV s^{-1}. However, there is no significant change in the shape and position of the redox peaks in the scan rate range of 5 mV s^{-1} to 100 mV s^{-1}, suggesting that (i) the *as*-prepared alloy is favorable for fast redox reaction and (ii) the electrode has a relatively low resistance due to good interconnection between the electrode active materials and contact with the current collector [25].

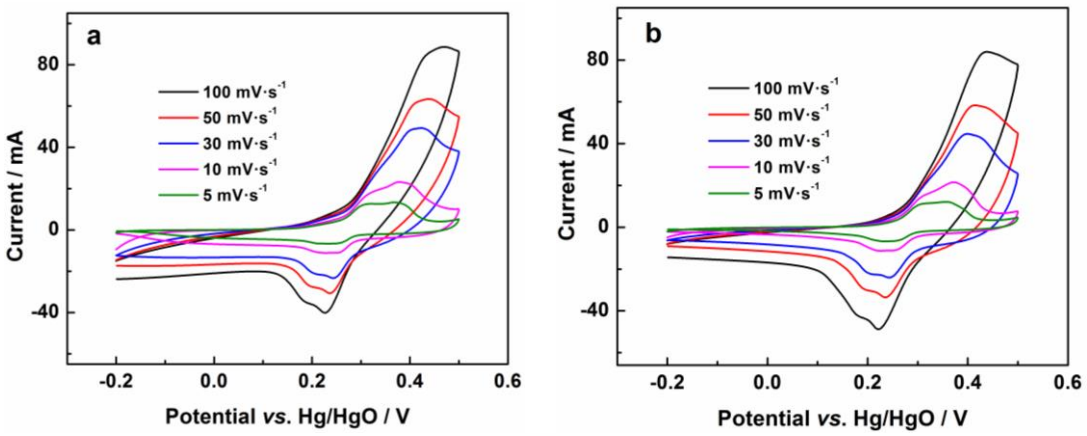

Figure 5 Cyclic voltammograms of NiCoB (a) and NiCoBP (b) electrodes at various scan rates.

The galvanostatic charge-discharge profiles of NiCoB and NiCoBP alloys are shown in Figure 6(a). The figure shows potential plateaus at ca. +0.25 and +0.35V *vs.* Hg/HgO, which is in good agreement with the CV results. The specific capacitance values derived from the discharge curves were calculated using following equation:

$$C = \frac{Q}{V} = \int \frac{i \bullet t}{V \bullet m} \qquad (1)$$

where i is the sampled current, t is the sampling time span, V is the total potential deviation of the voltage window, and m is the mass of the active electrode material. The specific capacitance of NiCoB and NiCoBP is 1895.2 and 1925.6 F g^{-1}, respectively. The rate capability testing of NiCoB and NiCoBP alloys was carried out at current densities ranging from 50 mA g^{-1} to 6 A g^{-1}. Figure 6(c) and 6(d) show that specific capacitances decreased as the current density increased, which is in excellent agreement with reported observations in the literature for Ni and Co based hybrids [25, 26]. As shown in Figure 6(b), the specific capacitance of NiCoB drops from 1895.2 to 875.0 F g^{-1} when the current density increases from 50 mA g^{-1} to 10 A g^{-1}. The capacitance decreases with increased current due to the ohmic losses and diffusion constraints. From 50 mA g^{-1} to 10 A g^{-1}, the specific capacitance of NiCoBP decreases from 1,925.6 to 895.2 F g^{-1}, corresponding to a 46.5% retention of the initial capacitance. In the case of NiCoB, it was found that the capacitance retention was 46.0 % at a current density of 10 A g^{-1},. Although the BET surface area of NiCoB is higher than that of NiCoBP, both alloys show similar specific capacitances and capacitance retentions, due to the presence of phosphorous.

Amorphous alloys consisting of solid particles with irregular shape have attracted a

great deal of attention due to their interesting intrinsic properties, such as short-range order, long-range disorder and highly unsaturated sites [9]. It is well known that Faradaic redox reactions occur in a thin surface layer of the electrode active materials [27]. On the surface of amorphous and mesoporous alloys, there are more unsaturated sites available for the redox reactions and the mesoporous structure can also facilitate rapid ion movement. Therefore, the amorphous and mesoporous alloys should present better electrochemical performance as materials for *pseudo* capacitors. The specific capacitances at 1 A g^{-1} for the *as*-prepared NiCoB and NiCoBP alloys were found to be 1,342.0 and 1,350.4 F g^{-1}, respectively; these are much higher than that of a hybrid nanostructure made of ultrathin $NiCo_2O_4$ nanosheets (899 F g^{-1} at 1 A g^{-1}) [25], and $NiCo_2O_4$ hollow spheres (1141 F g^{-1} at 1 A g^{-1}) [28]. The comparison with crystalline $NiCo_2O_4$ nano-structured alloys shows that the amorphous and mesoporous structure can significantly improve the specific capacitance.

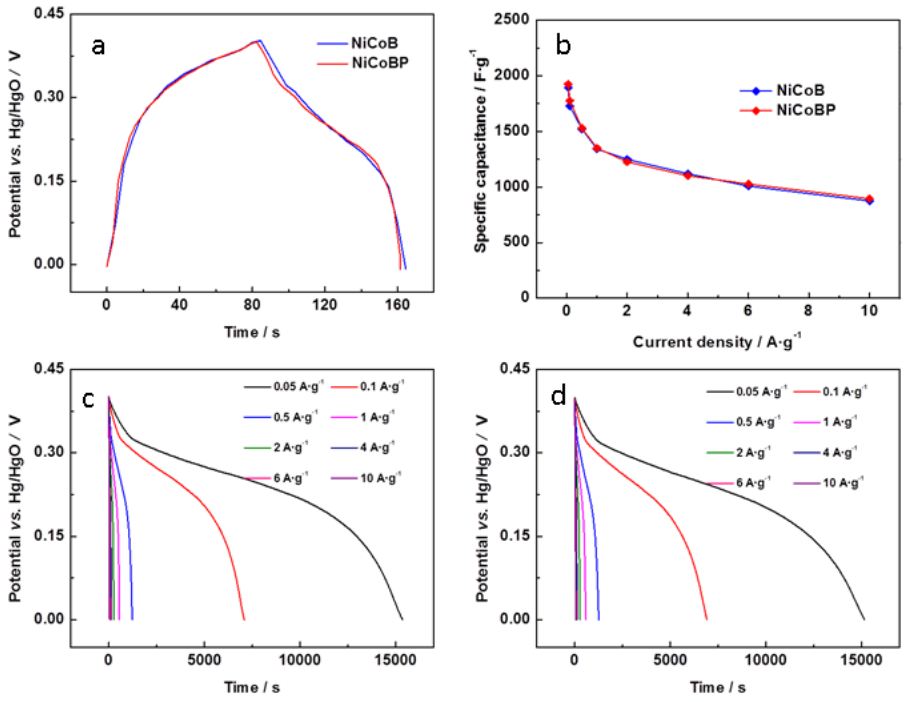

Figure 6 (a) galvanic charge-discharge curves of CV curves of NiCoB and NiCoBP; (b) specific capacitance with varying current density; (c) discharge curve with varying current density of NiCoBP; (d) discharge curve with varying current density of NiCoB

The long-term cycle stability and capacitance retention of NiCoB and NiCoBP alloys was evaluated over 1,000 continuous charge-discharge cycles at a current density of 6 A g^{-1} (Figure 7). It can be seen from the figure that the specific capacitance of NiCoB alloys gradually decreases from 1,013.5 F g^{-1} in the first cycle at 6 A g^{-1} to 586.7 F g^{-1} after 1,000 cycles. The capacitance retention for the NiCoB alloy is 57.9 % of the highest capacitance after 1,000 cycles and maintained close to 100% coulombic efficiency. In the case of the NiCoBP alloy, a much lower capacitance fade was observed, the specific capacitance slowly decreased from 1,035.1 to 879.8 F g^{-1} after 1,000 cycles, which corresponded to a capacitance retention of 84.5 %. The results clearly demonstrate that *as*-prepared mesoporous and amorphous NiCoBP possesses promising cycling stability. Although both of the alloys possess similar structures and specific capacitances, NiCoBP is much more stable than NiCoB in terms of cycling stability. Since both alloys were synthesized by a similar procedure, it is clear that the enhanced cycling stability is due to the presence of phorphorous. Phosphorous, a non-metallic element, has a large influence over the electronic state of metal elements; this often has beneficial results, for example, enhanced catalytic activity [29, 30]. In our previous works [16, 31, 32], it was found that introducing phosphorus into metal alloys can form stable amorphous

structures. Since NiCoB and NiCoBP alloys were synthesized under the same conditions and possess almost similar specific capacitances, it could be concluded that the high cycling stability of NiCoBP benefits from the stable amorphous structure which is formed in NiCoBP due to the presence of phosphorous.

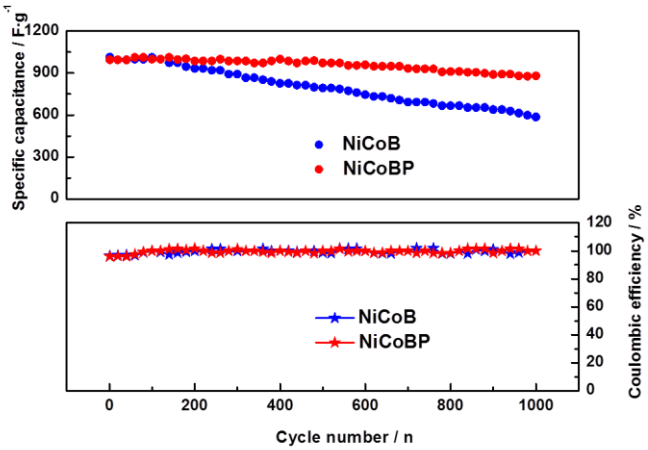

Figure 7 Cycling performance of NiCoB and NiCoBP over 1000 cycles at 6 A g^{-1}.

Conclusions

Mesoporous and amorphous NiCoBP alloys with high surface areas as cathodes for asymmetric supercapacitors were synthesized using a low cost solid-liquid interface-mediated method at room temperature. The *as*-prepared NiCoBP alloy exhibited high specific capacitance of 1,350.4 F g^{-1} at 1 A g^{-1} and a high capacity retention rate of 66 % when the discharge current density increased from 1 to 10 A g^{-1}. A good cycling stability with 84.5% of the initial capacity retention after 1,000 cycles at 6 A g^{-1} was achieved. It was found that the superior supercapacitive performance was mainly attributed to the mesoporous and amorphous structures formed in the NiCoBP alloy, providing highly unsaturated sites for the redox reactions as well as

facilitating fast charge transport. This novel method could be used to synthesize many other amorphous electroactive materials with high surface area for supercapacitors.

Acknowledgment

The authors would like to thank the National Natural Science Foundation of China (21363022, and 51362027) and JCYJ20140418095735600 for financially supporting this work.

References

[1] Y. Li, Z. Li, P.K. Shen, Adv Mater, 25 (2013) 2474-2480.
[2] R. Jiang, T. Huang, J. Liu, J. Zhuang, A. Yu, Electrochimica Acta, 54 (2009) 3047-3052.
[3] S. Maiti, A. Pramanik, S. Mahanty, ACS Applied Materials & Interfaces, 6 (2014) 10754-10762.
[4] M. Qorbani, N. Naseri, A.Z. Moshfegh, ACS Applied Materials & Interfaces, 7 (2015) 11172-11179.
[5] Y.-M. Hu, M.-C. Liu, Y.-X. Hu, Q.-Q. Yang, L.-B. Kong, W. Han, J.-J. Li, L. Kang, Electrochimica Acta, 190 (2016) 1041-1049.
[6] A.T. Chidembo, S.H. Aboutalebi, K. Konstantinov, C.J. Jafta, H.K. Liu, K.I. Ozoemena, RSC Adv., 4 (2014) 886-892.
[7] Y. Zhao, Y. Meng, P. Jiang, Journal of Power Sources, 259 (2014) 219-226.
[8] Y. Ma, H. Li, H. Wang, S. Ji, V. Linkov, R. Wang, Journal of Power Sources, (2014).
[9] W. Zhang, Y. Tan, Y. Gao, J. Wu, B. Tang, J. Zhao, RSC Advances, 4 (2014) 27800.
[10] H. Wang, Y. Ma, R. Wang, J. Key, V. Linkovb, S. Ji, Chemical Communications, 51 (2015) 3570-3573.
[11] Y.D. Wang, X.P. Ai, Y.L. Cao, H.X. Yang, Electrochemistry Communications, 6 (2004) 780-784.
[12] C. Wu, Y. Bai, F. Wu, X. Wang, J.-y. Lu, C. Qiao, Electrochemistry Communications, 11 (2009) 2173-2176.
[13] H.X. Yang, Y.D. Wang, X.P. Ai, C.S. Cha, Electrochemical and Solid-State Letters, 7 (2004) A212.
[14] Y. Ma, H. Wang, H. Li, J. Key, S. Ji, R. Wang, RSC Advances, 4 (2014) 20722-20728.
[15] Y. Cao, W. Zhou, X. Li, X. Ai, X. Gao, H. Yang, Electrochimica Acta, 51 (2006) 4285-4290.
[16] Y. Ma, H. Li, H. Wang, X. Mao, V. Linkov, S. Ji, O.U. Gcilitshana, R. Wang, Journal of Power Sources, 268 (2014) 498-507.
[17] F. Reincke, S.G. Hickey, W.K. Kegel, Vanmaekelbergh，Daniel, Angew. Chem. Int. Ed. , 43 (2004) 458-462.
[18] R. Wang, Y. Ma, H. Wang, J. Key, S. Ji, Chemical Communications, (2014).
[19] X. Wang, Q. Peng, Y. Li, Acc. Chem. Res., 40 (2007) 635-643.
[20] J. Guo, Y. Hou, C. Yang, Y. Wang, H. He, W. Li, Catalysis Communications, 16 (2011) 86-89.
[21] N. Passe-Coutrin, S. Altenor, D. Cossement, C. Jean-Marius, S. Gaspard, Microporous and Mesoporous Materials, 111 (2008) 517-522.
[22] X. Wang, X. Han, M. Lim, N. Singh, C.L. Gan, M. Jan, P.S. Lee, The Journal of Physical Chemistry C, 116 (2012) 12448-12454.
[23] V. Gupta, S. Gupta, N. Miura, Journal of Power Sources, 175 (2008) 680-685.

[24] H. KuanXin, Z. Xiaogang, L. Juan, Electrochimica Acta, 51 (2006) 1289-1292.
[25] G. Gao, H.B. Wu, S. Ding, L.M. Liu, X.W. Lou, Small, 11 (2015) 804-808.
[26] W. Kong, C. Lu, W. Zhang, J. Pu, Z. Wang, J. Mater. Chem. A, 3 (2015) 12452-12460.
[27] D. Choi, G.E. Blomgren, P.N. Kumta, Advanced Materials, 18 (2006) 1178-1182.
[28] L. Shen, L. Yu, X.Y. Yu, X. Zhang, X.W. Lou, Angew Chem Int Ed Engl, 54 (2015) 1868-1872.
[29] X. Xue, J. Ge, C. Liu, W. Xing, T. Lu, Electrochemistry Communications, 8 (2006) 1280-1286.
[30] W.D. King, J.D. Corn, O.J. Murphy, D.L. Boxall, E.A. Kenik, K.C. Kwiatkowski, S.R. Stock, C.M. Lukehart, The Journal of Physical Chemistry B, 107 (2003) 5467-5474.
[31] Y. Ma, H. Wang, W. Lv, S. Ji, B.G. Pollet, S. Li, R. Wang, RSC Advances, 5 (2015) 68655-68661.
[32] Y. Ma, R. Wang, H. Wang, V. Linkov, S. Ji, Physical Chemistry Chemical Physics, 16 (2014) 3593-3602.